JOURNAL OF MATERIALS SCIENCE 22 (1987) 3737–3744

Compressive fracture processes in an alumina–glass composite

ROY ARROWOOD*, JAMES LANKFORD
Southwest Research Institute, San Antonio, Texas 78284, USA

At atmospheric pressure, a commercial 85% alumina fails by granulation, breaking into small flakes and splinters with long dimensions parallel to the load axis. Replica transmission electron microscopy examination of polished surfaces on specimens loaded to 89% (or more) of the fracture stress reveals the formation of microcracks at crystal–glass interfaces subparallel to the load axis. Scanning microscopy of granulated samples indicates that pores in the material either initiate or channel the cracks which dissect the ceramic into small particles during granulation failures. Thus, the interpore spacing seems to be an important factor in the particle size distribution of the broken ceramic. In the faulting mode of failure, which occurs under confining pressure, the sliding faces of the ceramic are slickensided. However, most of the loose fracture particles do not display slickensides; in size and shape they resemble the powder produced by granulation failures. True "fault gouge" material, consisting of comminuted particles mashed together, tends to adhere to the fault faces. The gouge has a broad particle size distribution, including particles much finer than the interpore spacing of the ceramic. At the highest loading rate (0.81 sec^{-1}) under atmospheric pressure, the particles produced by granulation fracture are slickensided and show evidence of either localized melting or plastic grooving induced by friction between adjacent particles.

1. Introduction

As described in a companion paper [1], the compressive strength of an 85% alumina ceramic (AD-85, Coors Porcelain Company, Golden, Colorado) increases by 38%, from 2140 to 2950 MPa, upon application of just 41 MPa of hydrostatic confining pressure. The increase in strength is accompanied by a change of failure mode from granulation to faulting. Above 41 MPa pressure, the increase of strength with increased pressure is much more gradual. Under atmospheric pressure (0.10 MPa), varying the strain rate from 0.11×10^{-3} to 0.81 sec^{-1} increases the strength from 2140 to 2430 MPa. A previous study of a > 99% alumina ceramic has revealed a similar effect of confining pressure on compressive fracture stress [2]; in that investigation, all tests were at a strain rate of about 10^{-4} sec^{-1}, and no micrography of the failed samples was reported. An extensive study [3, 4] of rate and temperature effects on the fracture of Lucalox (99.9% alumina; General Electric Company, Lamp Glass Division, Cleveland, Ohio) at atmospheric pressure also provides information on the behaviour of nearly pure alumina ceramics, which can be used to make informative comparisons with the behaviour of the AD-85. The work reported here has examined the effects of confining pressure and strain rate on the compressive strength and failure modes of AD-85, an alumina ceramic with a thick, continuous glassy phase. Elsewhere [1] we describe the effects of pressure and rate on the compressive strength. In this report, we describe microscopic observations that furnish clues to the mechanisms of failure of AD-85 alumina in compression.

2. Experimental methods

The compression test procedure is described elsewhere [1]. Briefly, right circular cylinders 6.36 mm in diameter by 13.36 mm long were compressed axially inside a pressure vessel which permits application of a hydraulic confining pressure to the cylindrical surface. All of the tests were performed at room temperature. The confining pressure range of the experiments performed to date was 0.10 to 340 MPa, and the compression rates varied from 0.11×10^{-3} to 0.81 sec^{-1}. Heat-shrinkable Teflon (polytetrafluoroethylene) tubing, shrunk around the specimen and the platens, isolated the ceramic from the pressure-transmitting fluid, and also retained the broken fragments so that they could be retrieved for examination. However, in the atmospheric-pressure tests, the rupture of the ceramic was violent enough to tear the Teflon, so that only part of the granulated ceramic remained in the jacket.

Specimens compressed under a confining pressure of 41 MPa or more failed by a distinctively different mode, i.e. by the formation of a fault at an angle of approximately 32° to the compression axis. Compression was continued until the specimen had experienced a total shortening of as much as 24%, in order to generate some information on the compressive load-bearing capacity of the fractured material

*Present address: Mechanical Engineering, University of California, Irvine, California 92717, USA.

0022–2461/87 $03.00 + .12

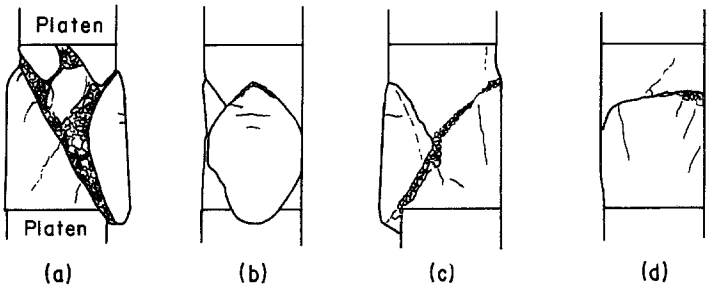

Figure 1 Sketch of AD-85 specimen after 17% shortening at 1.1×10^{-3} sec^{-1} strain rate with 165 MPa confining pressure. Views at (a) 0°, (b) 90°, (c) 180°, (d) 270°.

(reported elsewhere [5]). After retrieval from the test apparatus, the specimens were sketched and photographed to record the configuration of the fault and subsidiary fractures; then, in some cases, the Teflon jacket was carefully cut away and the gouge (powdered material) from the fault was sieved to obtain a particle size distribution curve. Because of the small amount of powder available, no more than five sieves were used. The powder caught on each sieve was weighed to the nearest tenth of a milligram. Some loss of powder was unavoidable, but in the sieving process less than one per cent of the mass of the powder was lost.

In order to reveal the processes preceding failure, some samples were ground and polished to produce a flat surface parallel to the cylinder axis prior to compression testing. These specimens were loaded to a high fraction of the mean failure stress, unloaded quickly, and preserved for microscopic examination of the flat. By this means pre-failure microcracking processes have been documented in Dresser basalt [6] and Lucalox alumina [7], and sintered α-SiC [8]. In the present material, microcracks could not be detected by scanning electron microscopy, even after loading to 93% of the fracture stress. Therefore, acetate replicas were taken from the flats on two specimens and shadowed with palladium to permit a search for microcracks by transmission electron microscopy. Replicas were taken not only in the unloaded state, but also during reapplication of about half the nominal failure stress in order to open up any tensile microcracks which might be present.

3. Results and discussion

3.1. Failure modes

When compressed under ambient pressure, AD-85 invariably failed by shattering into small particles. No end-cones formed, and the particles which remained in place in the ruptured Teflon jacket were flakes or splinters with long axes parallel to the compression direction. This observation is evidence of failure by the growth of tensile microcracks in planes parallel to the compression axis, a well-documented mode of failure of ceramics and rocks at low confining pressures [9–12]. Smaller particles tend toward a more equidimensional shape. Because the specimen is reduced to a powder resembling granulated sugar, this failure mode will be referred to as granulation. In contrast, specimens tested at hydrostatic pressures of 41 MPa or more failed by formation of a fault. Continued compression of the sample was accommodated by sliding of the specimen halves along the fault plane, and a "gouge" of powdered ceramic was produced along this sliding surface. Fig. 1 is a sketch of a specimen which failed by faulting. It is clear that the fault is not truly planar, and that there is a second diagonal fracture symmetrically arranged with respect to the major fault, but not so well developed. Numerous other fractures are visible.

As described in the companion paper [1], the loading curves are straight at atmospheric pressure, but exhibit a slight deviation from linearity (concave toward the strain axis) under pressure. The deviations may result from plasticity of the glass phase or from microcracking prior to gross failure. In order to characterize the microcracking processes, two specimens with polished flats were loaded to high fractions of the fracture stress at 0.11×10^{-3} sec^{-1} and atmospheric pressure. One specimen was loaded to 89%, the other to 95% of the mean fracture stress and rapidly unloaded. Scanning electron microscopy did not reveal any microcracks on the polished flat, despite indications from acoustic emission monitoring that numerous apparent microcracking events had taken place. Accordingly, replicas were made for transmission microscopy. A first set of replicas were taken with the specimens in the unloaded state, and a second set under a load equal to 47% of the mean fracture stress, in the hope that the load would open the microcracks and make them more evident in the replica. The specimen previously loaded to 95% of the fracture stress shattered after less than two minutes at the 47% stress level, which is an indication that microcracking had indeed been induced by the initial loading.

Fig. 2 is a transmission micrograph of one replica of

Figure 2 Shadowed replica of polished surface of a specimen after loading to 1812 MPa at 0.10 MPa confining pressure and a strain rate of 1.1×10^{-4} sec^{-1}. Arrows indicate compression direction.

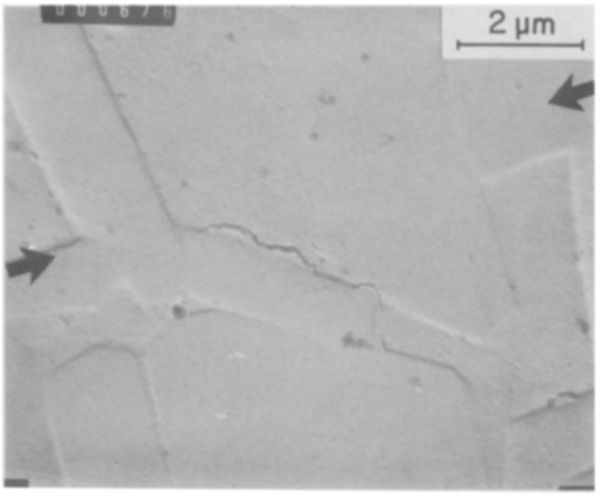

Figure 3 Enlarged replica of a microcrack. Same specimen as Fig. 2. Arrows indicate compression direction.

a specimen loaded to 89% of the failure stress. The alumina crystallites stand in relief because they resist polishing more than the glass does. In the lower right quadrant of the picture is the case of a pore. Wavy black lines, which are interpreted as replica indications of microcracks, occur in several places in the field of view. They typically lie along crystallite–glass interfaces, in orientations subparallel to the compression axis. The large black feature adjacent to the pore may be a flap of replica material which has pulled out of the pore. It is clear from the examination of several replicas that by 89% of the fracture load pervasive microcracking has taken place. Such cracks do occur around pores, but they also occur abundantly away from the pores, usually along crystal–glass interfaces. Fig. 3 enlarges such a crack, which is typical in that it appears that most of its length lies not in the interface, but within the glass a slight distance away from the interface.

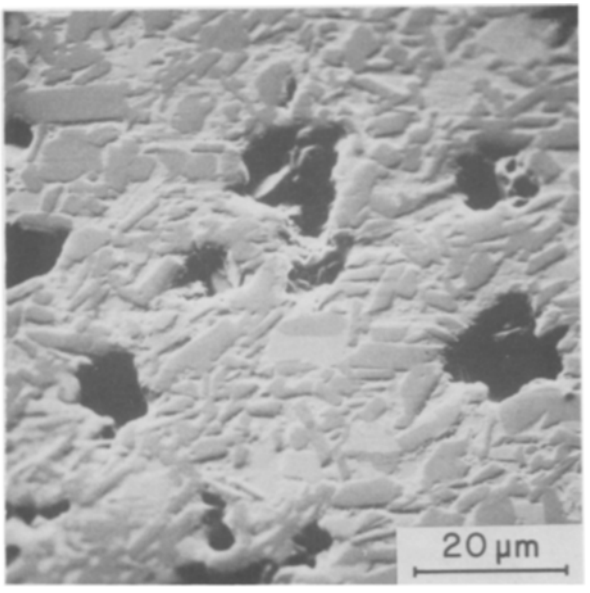

Figure 5 Scanning electron micrograph of polished sample loaded to 2417 MPa at 1.1×10^{-3} sec^{-1}, with 48.9 MPa confining pressure. The compression axis is horizontal.

3.2. Granulation failures at low rates

When loaded to failure at atmospheric pressure, this ceramic fails by granulation. Fig. 4 is a scanning electron micrograph of fragments of a specimen loaded at 0.11×10^{-2} sec^{-1}. The flake-like shape of most of the larger particles is evident. Also, there are few particles smaller than 50 μm. This size limit is considerably larger than the alumina crystallite size of 3 to 25 μm, but compares well with the interpore spacing in this ceramic (Fig. 5). The smaller particles, upon closer examination, turn out to contain many crystallites. Furthermore, swarms of microcracks cut through pores that lie exposed on the surfaces of the ceramic particles (Fig. 6). Corners of the angular particles are often occupied by pores.

The replica work indicates that the first microcracks form at or near crystal–glass interfaces which lie nearly

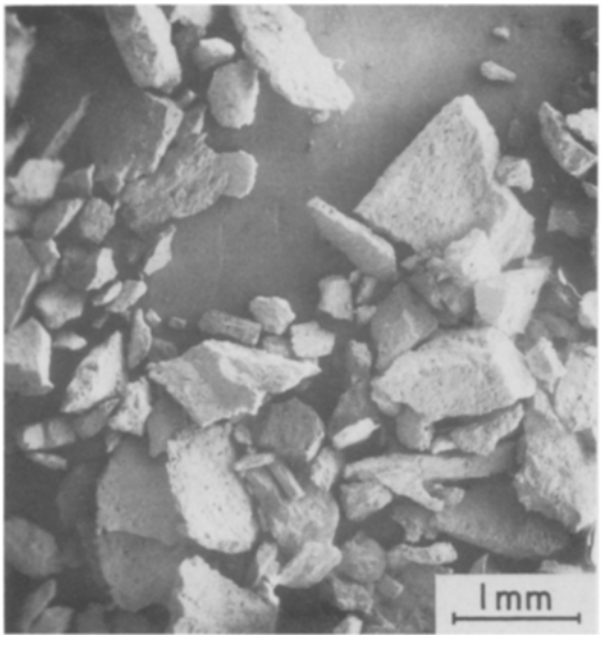

Figure 4 Fragments of a specimen compressed at a rate of 1.1×10^{-3} sec^{-1} under atmospheric pressure.

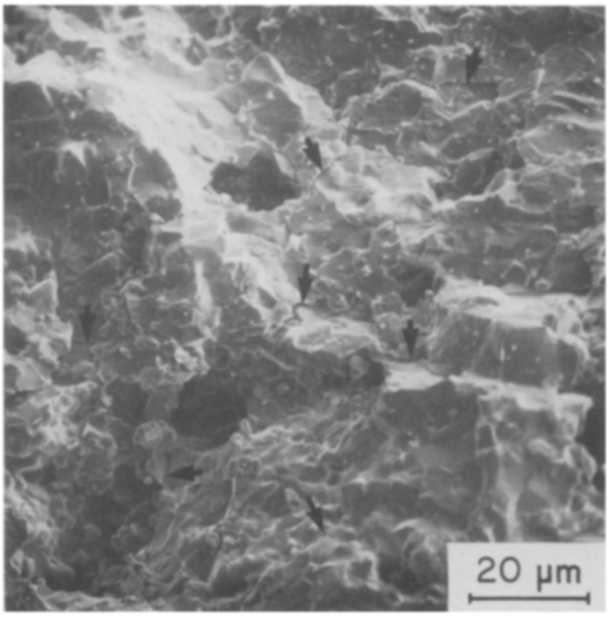

Figure 6 Microcracking (arrows) around pores on the surface of a fragment shown in Fig. 4.

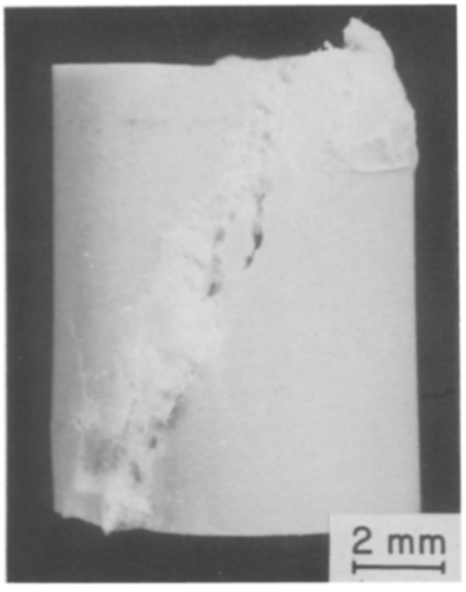

Figure 7 A specimen compressed beyond failure at 1.1×10^{-3} sec^{-1} under a confining pressure of 83 MPa.

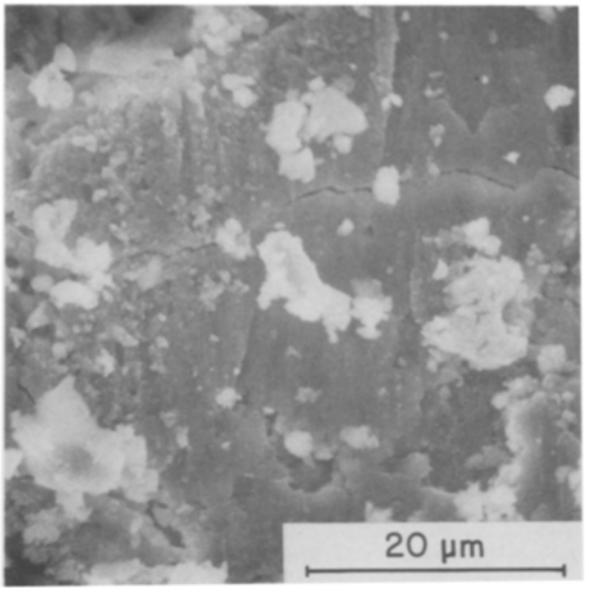

Figure 9 Slickensides on fault surface.

parallel to the compression axis. These precursor cracks do not show a strong propensity to emanate from pores, but rather tend to be uniformly distributed. On the other hand, the (larger) cracks observed within particles of the fractured ceramic are most abundant around pores. Also, the tendency for particles to have pores at their corners, and the similarity of the smaller particle sizes to the interpore spacing, support the argument that the porosity plays an important role in the disintegration of the ceramic once the cracking becomes unstable.

3.3. Faulting failures

Fig. 7 depicts a faulted sample after removal of its jacket. This sample was wrapped (under the jacket) with a layer of soft Teflon tape of the type used in plumbing to seal threaded connections. Under pressure, the Teflon intruded into the pores and the fault, an undesirable complication, and this procedure was not used in later tests. However, the thin layer of Teflon on the surface did bind the failed sample together so that it was possible to remove the jacket without demolishing the sample. The gouge layer is clearly visible in this photograph.

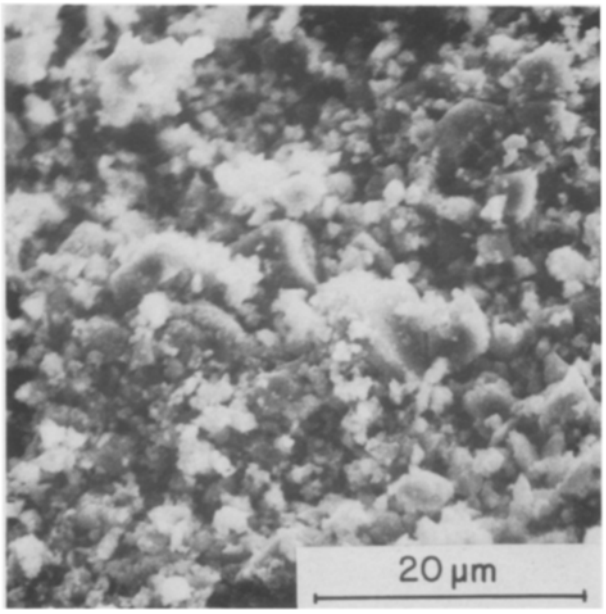

Figure 8 Compacted gouge adhering to sliding surface of a sample which failed by faulting at 1.1×10^{-2} sec^{-1} (confining pressure 84.7 MPa).

When a faulted sample is separated so that the faces of the fault may be examined in the SEM, it is found that part of the fault area is covered with a layer of compacted gouge (Fig. 8). The size distribution of this material is broad, and many of the larger particles appear to be aggregates of small particles that have been compacted together. This type of gouge is to be expected as a product of faulting, in which particles caught between the faces are sheared and compacted. Other areas of the fault surface are slickensided (Fig. 9), crusted with a smooth surface layer of smeared material which bears indistinct striations in the sliding direction and cracks approximately perpendicular to the striations. Fig. 10 displays the fragments of a faulted specimen after removal from the jacket and sieving. The finest (less than 150 μm) fragments constitute less than 3% of the whole specimen. The particle size distribution of a sample tested at 85 MPa pressure is plotted in Fig. 11. Since there are few particles larger than 2 mm (a significant fraction of the specimen size), the cumulative percentages are computed on the basis of the amount of material finer than 2 mm. It is this finer material that makes up the gouge. Particles smaller than 45 μm make up less than 1% of the mass of the fines; the fiftieth percentile particle size is about 500 μm.

Although the compacted gouge which adheres to the sliding surfaces is distinctive in particle size range and shapes, most of the loose powder recovered from faulted samples is comparable in particle size and shape to the powder produced in granulation failures at ambient pressure. This powder may have formed in the central region of the specimen by tensile microcracking prior to fault development [13]. Another

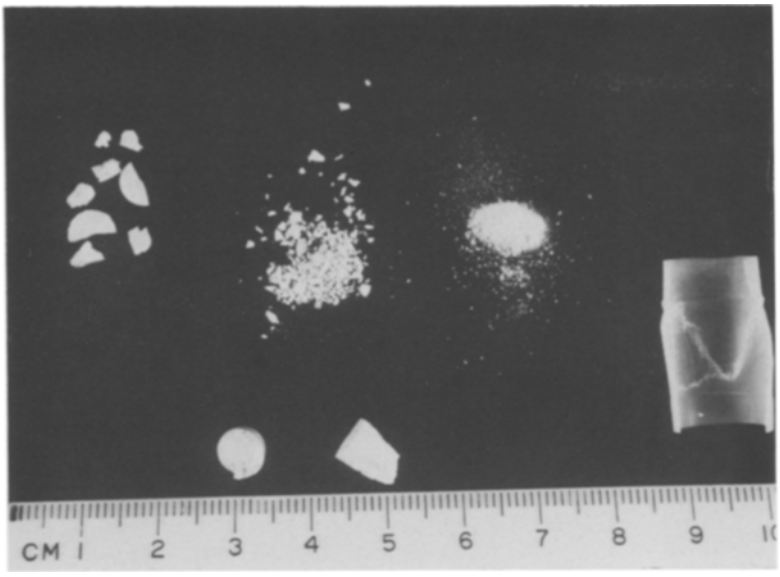

Figure 10 Fragments of sample which failed by faulting at 1.1×10^{-2} sec^{-1} under a confining pressure of 84.7 MPa. In the upper part of the photograph, from left to right, are the particles in the $> 2000\,\mu$m, 150 to 2000 μm, and $< 150\,\mu$m size fractions. Below these, next to the scale, are the two end-pieces with fault surfaces and, to the right, the Teflon jacket.

explanation is that it may have detached from the fault walls by tensile cracking due to the shear tractions on the walls of the fault; in a study of microfracture processes in rock drilling, Zeuch *et al.* [14] have observed such purely tensile cracking beneath a cutting tool. Fig. 7 captures a large chip in the process of detachment from the fault wall. The chip is breaking free by the combination of an axial (predominantly tensile) crack and a mixed-mode crack segment approximately parallel to the fault plane. Shear displacement is evident on at least part of the crack, and thus it would seem that this type of particle should display some evidence of shear-mode cracking. Vague, parallel lineations are sometimes discernable on the larger particles from the fault zone, but not well-developed slickensides. However, the fracture surface is of the "mantled" type rather than the transgranular type predominant in tensile microfractures (see Section 3.5). Fig. 12 shows an example of one of the larger particles from the fault zone. Fig. 13 enlarges a pore at a corner of the particle, with cracks radiating from it. There is no evidence of slickensiding on the particle.

3.4. Granulation failures at high loading rate

At a strain rate of 0.81 sec^{-1}, under atmospheric pressure, the failure is by granulation, but scanning microscopy of the fragements reveals features on the particle surfaces that are not present at 0.11×10^{-2} sec^{-1} or less. Parts of the surfaces of most particles are covered by slickensides, even though no confining pressure was applied (Fig. 14a). Further enlargement of slickensided areas reveals features which may indicate highly localized melting. One such feature is shown in Fig. 14b; it may be interpreted as a droplet of molten glass smeared into an elongated shape between two particles sliding over each other. Yust and Crouse [15] reported similar features resulting from melting at particle impact sites on alumina bricks. However, their samples were preheated to 470° C and the particle impact velocities were 24.4 m sec^{-1}; in contrast, the present experiment was at room temperature with a ram speed of about 0.01 m sec^{-1}. Moreover, the appearance of the surface

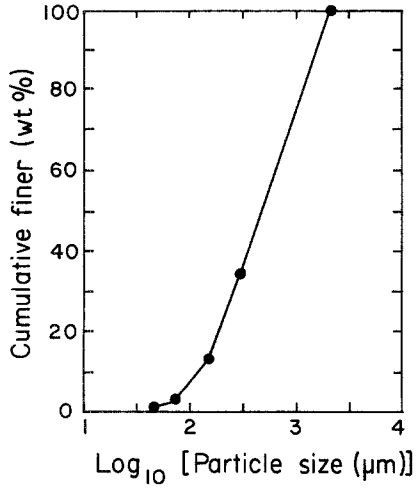

Figure 11 Particle size distribution of the < 2 mm fraction of a faulted specimen compressed to 19% shortening at 1.1×10^{-3} sec^{-1} under 165 MPa pressure.

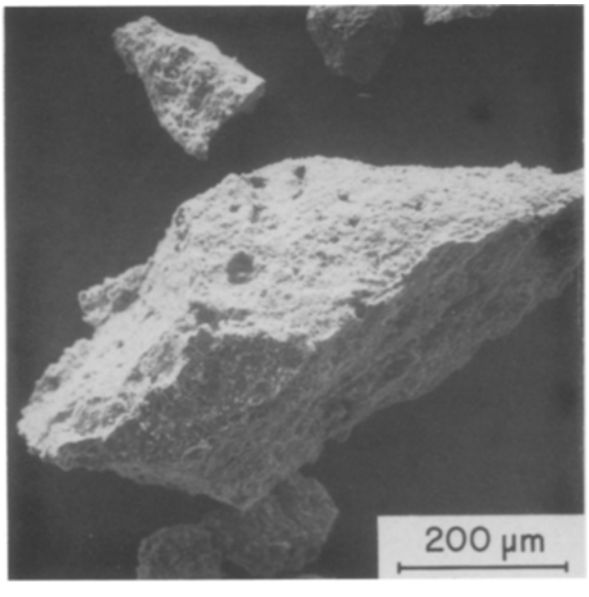

Figure 12 A large particle from the gouge layer in a faulted specimen.

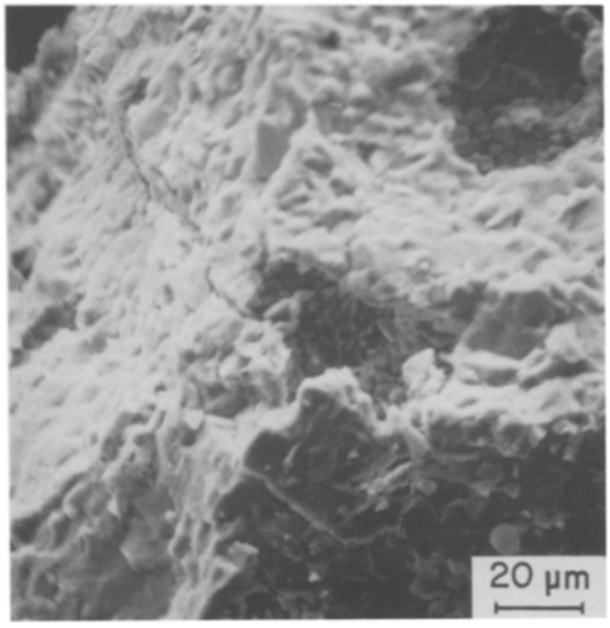

Figure 13 Enlargement from Fig. 12, showing cracking around a pore at a corner of the particle.

features does not rule out their production by plastic grooving without melting. Consistent with this latter explanation is the observation that their width (about 0.6 μm or less) is below the critical scratch width for cracking in a soda–lime glass [16]. However, in dealing with glasses and with glass–crystal composites such as AD-85, the distinction between shear-induced melting and plastic grooving may be litttle more than semantics: glass has no melting point, but instead shows a strong, continuous decrease in viscosity as the temperature rises.

3.5. Comparison with a glass-free alumina

Comparison of the compression failure of AD-85, containing a prominent glassy phase, to that of essentially glass-free Lucalox [3, 4, 7, 17] reveals many differences. The microstructure of Lucalox consists of equidimensional 20 to 30 μm alumina grains, with a uniform distribution of round pores situated on grain boundaries. The pores are up to 7 μm in diameter and occupy about 1% or less of the volume of the ceramic. Thus, the outstanding differences between Lucalox and AD-85 are: (i) the presence of a thick, continuous glass phase in AD-85: (ii) smaller average alumina grain size in the AD-85, although the maximum grain sizes are fairly comparable; and (iii) the presence of 11% porosity in AD-85 as opposed to about 1% in Lucalox, and the irregular shape, large dimensions (up to 60 μm) and clustered distribution of pores in the AD-85.

In Lucalox, twinning and twin-initiated microcracking commences at about 50% of the compressive failure strength [17]. In AD-85, acoustic emission begins at about the same stress as in Lucalox (1500 to 1700 MPa), but this corresponds to 80% of the failure stress of the weaker AD-85. Although acoustic emission in Lucalox was shown to correlate with twinning and twin-initiated microcracking, there was no evidence that twinning was involved in microcracking of the AD-85. Twins were not detected in unfailed specimens by scanning microscopy or by transmission microscopy of replicas. A few twins were seen on fragment surfaces, but even after failure twinning is much less common than in Lucalox. This may be due to the more compliant glass phase shielding the corundum particles from high twinning stresses. Characteristic microcracking in the glass near crystallites is consistent with this interpretation. Thus, it apparently is a coincidence that the stress levels for microcrack initiation are similar in the two very different aluminas.

Microcracks in the Lucalox tend to have axial orientations and are quite straight, following twin boundaries, cleavage planes, and grain facets. In AD-85, the microcracks lie only approximately parallel to the compression axis, and they take sinuous paths through the glass near glass–crystal interfaces.

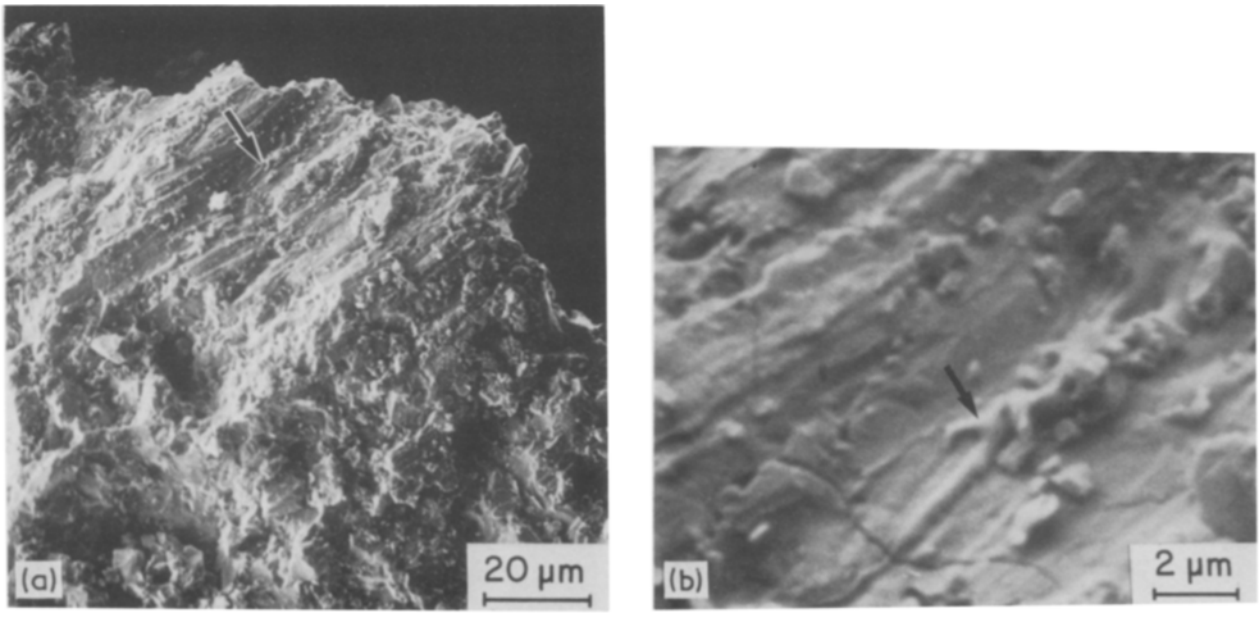

Figure 14 Slickenside area on a fragment of AD-85 from a specimen ruptured at 0.81 sec^{-1} under atmospheric pressure. Arrows in both micrographs indicate the same feature. (a) General view, (b) enlargement.

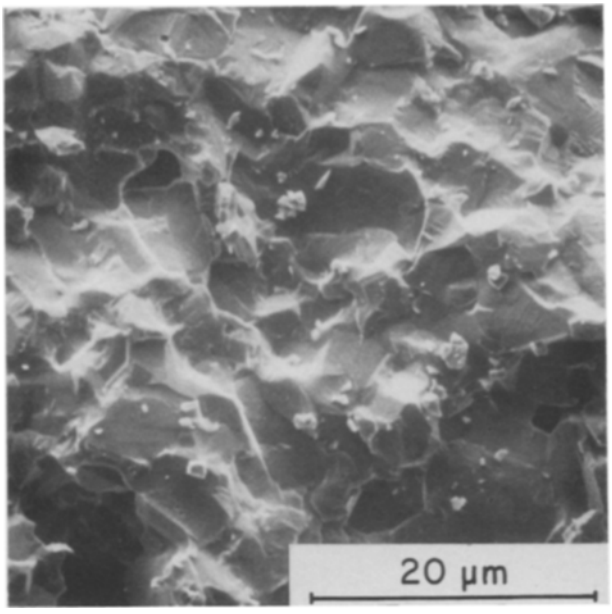

Figure 15 Surface of an AD-85 particle from a granulation failure at a strain rate of 1.1×10^{-3} sec^{-1} under atmospheric pressure.

Despite this pre-failure microcrack behaviour, the fragments of AD-85 compressed to failure at ambient pressure show extensive transgranular fracture (Fig. 15), with smooth to slightly conchoidal surfaces reminiscent of the transgranular fractures in Lucalox (Fig.16).

Cracking at the small, rounded pores in Lucalox is insignificant. In contrast, the rough-surfaced and larger pores of AD-85 seem to serve either as easy avenues of propagation for microcracks or as sites for the initiation of more damaging cracks. Based on present information, a plausible scenario for compressive fracture of AD-85 seems to be that in the initial, stable stage of cracking the glass phase protects the corundum grains from twinning and cleavage. But as loading continues the stress intensity around large pores becomes so great that stable mixed-mode microcracks in the glass can no longer accommodate the strain. At this point tensile fractures propagate from the pores, following paths that cut across crystallites as well as glass. The specimen granulates. Under confining pressure, the suppression of tensile fracture can be expected to permit further development of shear microcracks in the glass. Thus fragments of samples broken under confining pressure will display a "mantled" fracture surface as shown in Fig. 17. Since the fracture propagates mainly through the glass, it weaves between corundum crystallites. The crystals therefore find expression as a blocky topography, but it is not a sharp intergranular surface because the crystals are mantled by glass.

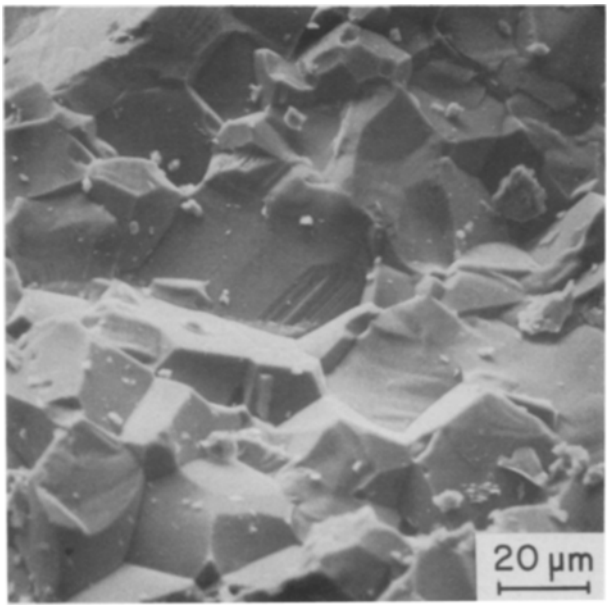

Figure 16 Surface of a particle of Lucalox which failed by granulation at 0.81 sec^{-1} under atmospheric pressure.

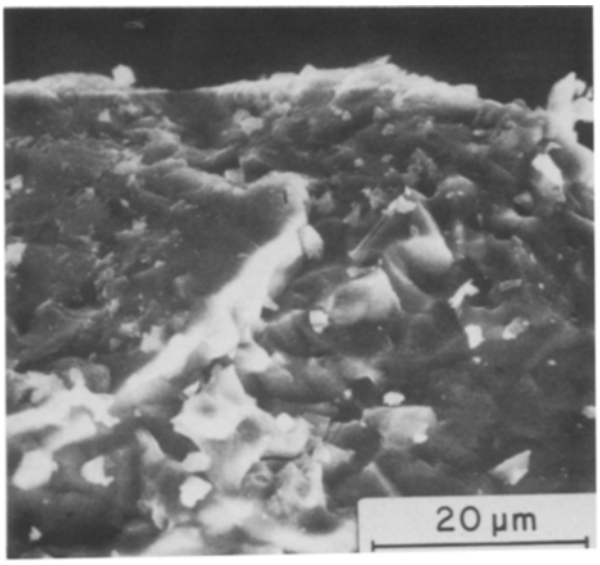

Figure 17 Surface of an AD-85 particle produced in faulting failure at a strain rate of 1.1×10^{-3} sec^{-1} under 84.7 MPa confining pressure.

Another interesting constrast between AD-85 and Lucalox is the presence of slickensides on particles of the former material fractured at 0.81 sec^{-1} with $P = 0.10$ MPa. Slickensides are absent on Lucalox particles produced under the same conditions (Fig. 15). The glass phase in AD-85 probably provides the material of which slickensides are made. Like other silicate glasses, this phase presumably has a highly temperature-sensitive viscosity which will tend to concentrate shear deformation in thin layers (slickensides) because of positive feedback between shear heating and fluidity.

4. Conclusions

1. Microcracks formed by loading AD-85 to about 90% of the fracture stress, at atmospheric pressure, are subparallel to the compression axis and lie in glass–crystal interfaces or within the glass adjacent to such interfaces.

2. Pores are important in the granulation fracture process, where they serve as crack initiation sites or as channels for propagating microcracks. The particle size distribution of the granulated material is influenced by the interpore spacing.

3. Comminuted material within faults in specimens failed under pressure includes not only very fine-grained gouge compacted on the fault faces, but also

a substantial proportion of coarser powder which resembles the products of granulation failures at atmospheric pressure. However, while ambient-pressure fracture surfaces are transgranular, fracture surfaces formed under confining pressure are mantled by a thin layer of glass.

4. At the highest rate ($0.81\,sec^{-1}$), the particles produced by ambient-pressure granulation are extensively slickensided due to interparticle friction.

Acknowledgements

We thank the Office of Naval Research and the Air Force Armaments Laboratory for support of this research.

References

1. R. ARROWOOD and J. LANKFORD, *J. Amer. Ceram. Soc.*, submitted.
2. H. C. HEARD and C. F. CLINE, *J. Mater. Sci.* **15** (1980) 1889.
3. J. LANKFORD, *ibid.* **16** (1981) 1567.
4. *Idem, Commun. Amer. Ceram. Soc.* **65** (1982) C-122.
5. R. ARROWOOD, *ibid.*, submitted.
6. J. LANKFORD, W. L. KO and U. S. LINDHOLM, "A Study of the Dynamic Strength and Fracture Properties of Rock," Final Report, Advanced Research Projects Agency Contract No. HO 220063 (1973).
7. J. LANKFORD, in "Fracture Mechanics of Ceramics", Vol. 5, edited by R. C. Bradt, A. G. Evans, D. P. H. Hasselman and F. F. Lange (Plenum, New York, 1983) p. 625.
8. *Idem. J. Amer. Ceram. Soc.* **62** (1979) 310.
9. *Idem, ibid.* **64** (1981) C33.
10. B. L. KARIHALOO, *Proc. R. Soc.* **A368** (1979) 483.
11. P. TAPPONIER and W. F. BRACE, *Int. J. Rock Mech. Min. Sci.* **13** (1976) 103.
12. R. L. KRANZ, *ibid.* **16** (1979) 23.
13. W. JANACH, *ibid.* **14** (1977) 209.
14. D. H. ZEUCH, D. V. SWENSON and J. T. FINGER, *Eos Trans. Amer. Geophys. Union* **63** (1982) 1110.
15. C. S. YUST and R. S. CROUSE, *Wear* **51** (1978) 193.
16. G. S. LOMDAHL and R. McPHERSON, *ibid.* **73** (1981) 205.
17. J. LANKFORD and D. L. DAVIDSON, in Proceedings of 3rd International Conference on Mechanical Behaviour of Materials, Vol. 3, Cambridge, UK, 20 to 24 August, 1979 (Pergamon, Oxford, 1980) p. 35.

Received 22 December 1986
and accepted 18 February 1987